Published paper
Lewis, R. and Dwyer-Joyce, R.S. Wear mechanisms and transitions in railway wheel steels. *Proceedings of the Institution of Mechanical Engineers, Part J: Journal of Engineering Tribology*, 2004, **218**(6), 467-478.

http://dx.doi.org/10.1243/1350650042794815

WEAR MECHANISMS AND TRANSITIONS IN RAILWAY WHEEL STEELS

R. LEWIS*, R.S. DWYER-JOYCE

Department of Mechanical Engineering, The University of Sheffield, Mappin Street, Sheffield, S1 3JD

*Corresponding author

ABSTRACT

The need to improve safety and reduce costs means new specifications are being imposed on railway wheel wear. These mean that more durable wheel steels are required. In order to develop such materials, a greater understanding is needed of the wear mechanisms and transitions occurring in wheel steels.

In this work twin disc wear testing has been carried out to study the wear characteristics of R8T railway wheel steel. The results have indicated that compared to previous wheel steels R8T offers greater wear resistance. Three wear regimes were identified; *mild*, *severe* and *catastrophic*. Wear rates were seen to increase steadily initially, then level off, before increasingly rapidly as the severity of the contact conditions increased. This paper is concerned with the form of the data and the reasons for the transitions.

Analysis of the contact conditions indicated that the first transition in the wear rate was caused by the change from partial slip to full slip conditions at the disc interface. Temperature calculations for the contact showed that the large increase in wear rates seen at the second wear transition may result from a thermally induced reduction in yield strength and other material properties.

This improved understanding will help in the progressing towards the aim of eventually attaining a wear modelling methodology reliant on material properties rather than wear constants derived from testing.

Keywords: railway wheel steel, wear mechanisms, wear transitions, wheel/rail wear

NOTATION

χ	Thermal diffusivity (m^2/s)
ε_{rad}	Emissivity of the disc steel
γ	Slip (percentage difference in disc surface speeds)
η_a	Dynamic viscosity of air (2×10^{-5} kg/m/s)
μ	Coefficient of friction
ρ_a	Density of air (km/m^3)
σ	Stefan-Boltzmann constant ($5.669\times10^{-8}W/m^2/K$)
a	Disc contact half width (m)
A	Contact area (m^2)
A_d	Area of a disc dissipating radiation energy (m^2)
b	Disc contact width (m)
C_p	Specific heat capacity of air (1 kJ/kg/K)
C_{ps}	Specific heat capacity of the wheel/rail steel (kJ/kg/K)
F_n	Normal load applied to twin discs (N)
k_a	Thermal conductivity of air (0.025 W/m/K)
k_s	Thermal conductivity of the wheel steel (W/m/K)
L	Peclet number
L_d	Disc circumference (m)
$\dot{q}$	Rate of heat supply per unit area (W/m^2)
$\dot{Q}_1$	Heat loss due to convection (W)
$\dot{Q}_2$	Heat loss due to conduction (W)
$\dot{Q}_3$	Heat loss due to radiation (W)
r	Disc radius at any point within the disc (m)

T Tractive force ($\mu \times p$) (N)

T_a Ambient air temperature (°C)

T_b Disc body temperature (°C)

T_f Flash temperature in disc contact (°C)

$\overline{T}_f$ Average flash temperature in disc contact (°C)

$\hat{T}_f$ Maximum flash temperature in disc contact (°C)

T_i Disc inner temperature (°C)

T_{tot} Total surface temperature (°C)

u_r Air velocity relative to the disc (equal to the disc surface speed) (m/s)

u_s Disc sliding speed (m/s)

U Velocity of contacting solid (m/s)

1 INTRODUCTION

New specifications are being imposed on railway wheel wear and reliability to increase the time between wheel reprofiling operations, improve safety and reduce total wheelset lifecycle costs.

In parallel with these requirements railway vehicle missions are changing due to:

- the need to operate rolling stock on track with low radius curves as well as the high radius curves on high speed line
- increasing speeds
- a decrease of track quality due to a reduction in maintenance

These are leading to an increase in the severity of the wheel/rail contact conditions **[1]**, which will increase the likelihood of wear occurring. Excessive wear can affect the dynamic behaviour of the railway vehicle and reduce ride comfort; impact upon the potential for derailment and reduce the integrity of the wheel material **[2]**.

In order to deal with these demands new wheel materials are being developed to give greater durability. To aid such development an improved understanding is required of the wear mechanisms and regimes apparent in wheel steels.

Previous work carried out to study the wear behaviour of railway wheel steels has led to the identification of a number of wear regimes **[3, 4, 5]**. Early tests demonstrated that two regimes existed **[3, 4]**. These were designated *mild* and *severe*. Later work led to the identification of a third regime, beyond the originally identified severe regime, designated *catastrophic* wear **[6]**. It was thought likely that wheel tread wear would fall within the mild regime while flange wear would be in the severe regime.

The regimes were characterised in terms of wear rate and wear debris. There was, however, no detailed analysis of the wear mechanisms occurring within the regimes and no understanding has been gained as to why the regimes exist. The aim of this work was, therefore, to study the wear rates and regimes of a railway wheel steel and examine in detail the wear mechanism evolution through the regimes as the severity of the contact conditions increases.

The main drawback in analysis tools that incorporate vehicle dynamics and wear modelling for predicting the evolution of wheel profiles **[7, 8, 9]**, is in the approach to wear modelling used in each. Previously developed wear models are taken, based on the Archard sliding wear model or a frictional work model, and used with wear coefficients taken from the literature. In each case the detail and accuracy of the dynamic and contact modelling far exceeds that of the wear modelling. Few investigations have been conducted to study the wheel material wear mechanisms or the suitability of the wear models being used. A clearer understanding of the wheel steel wear mechanisms will enhance the wear modelling procedures and enable improvements to be made to these tools.

A number of different techniques have been used for studying wear of railway wheel steels. Field measurements have been used in the past to study the causes of wheel and rail wear **[10]**. A large amount of data has also been gathered from simulated field experiments carried out on specially built test tracks **[11]**. Laboratory methods used range from, full-scale laboratory experiments **[12]** and scaled-down tests **[5]**, to bench tests using a twin disc set-up **[3, 4, 6, 13, 14]**. The twin disc approach was chosen for this work to offer greater control over experimental variables as well as the ability to test a wide range of materials at lower cost.

This work was carried out as part of the European Community funded project HIPERWheel. The main aim of this project was to develop an integrated CAE procedure for assessing wheelset durability taking into account damage mechanisms such as metal fatigue, rolling contact fatigue, wear and fretting. The purpose of this part of the study was to examine in detail the wear failure of the wheel material as a prerequisite to providing a model of the process.

2 EXPERIMENTAL DETAILS

2.1 Apparatus

The twin disc test machine used to carry out the testing is shown schematically in Figure 1. The original development of this machine and more recent work carried out to add a computer control system have been described previously **[15, 16]**.

The test discs are hydraulically loaded together and driven at controlled rotational speed by independent electric motors. The loading system is such that the discs are self aligning to avoid any stress concentrations at the contact edges; this is checked by inspection of the resulting wear track to ensure it is evenly distributed across the disc width. Shaft encoders

monitor the speeds continuously. A torque transducer is assembled on one of the drive shafts and a load cell is mounted beneath the hydraulic jack. The slip ratio required is achieved by adjustment of the rotational speeds. All data is acquired on a PC, which is also used for load and speed control.

2.2 Disc Specimens

The discs used during the testing were cylindrical and were cut from R8T wheel rims and UIC60 900A rail sections. They were machined to a diameter of 47mm with a contact track width of 10mm (see Figure 2). The contact surfaces were ground to achieve an average roughness of 1μm. Wheel specimens were drawn from the wheel rim parallel, and as close as possible, to the outer surface. Both disks are chamfered to avoid stress concentrations at the edges.

2.3 Experimental Procedure

Wear tests were carried out using the wheel disc as the driving disc and rail disc as the braking disc, as shown in Figure 3. A nominal disc rotational speed of 400rpm was used in the tests. An environment chamber enclosed the discs and air cooling was provided to both.

Suction was provided to remove wear debris for analysis. Wear measurement was determined by mass loss from the discs, measured before and after tests and at intervals during initial tests to determine the number of cycles required to reach steady state wear.

Tests were carried out varying contact pressure and slip to obtain wear data over a range of contact conditions. A test was included to determine the effect of absolute disc velocity. Test conditions used are shown in Table 1.

3 RESULTS

3.1 Progression of Wear

In the initial test carried out, wear measurements were taken periodically to establish the progression of wear and determine the number of cycles required to reach a steady state wear rate (see Figure 4). Data is included from a previous test carried out on the twin disc machine using W8A wheel material and BS11 rail. As can be seen the new R8T wheel steel wear rate is approximately 30% of the W8A wear rate, while rail wear is unaffected.

There appears to be an initial incubation period where wear rates are low. Often in wear situations there is an initial high wear rate associated with early running in as roughness and misalignments are worn out. In this instance that low initial wear rate is probably caused by the build-up of plastic strain in the surface. Once a threshold has been reached wear starts to take place. In all cases a steady wear rate is reached after 20000 cycles. In previous twin disc testing on the machine used for these tests **[17]** shear strain measurements 0.2mm below the surface of the discs indicated that after around 20000 cycles the strain accumulation rate reached its maximum and plateaus, explaining the subsequent constant wear rate.

The hardness values for the materials compared in Figure 4 are given in Table 2. These offer no obvious explanation for the difference in wear rates observed. It is possible that work hardening rate may play a role and it may be significant that the R8T and 900A materials are of similar hardness.

3.2 Wear Rates

Plotting the results from the tests carried out at constant load (1500MPa) shows that, at low values of slip, the wear rate (in mass loss/distance rolled) is approximately a linear function of slip (see Figure 5). Maintaining slip and increasing the load led to a rise in the wear rate and decreasing load led to a fall in the wear rate.

Varying absolute disc velocity while maintaining slip had little effect on the wear rate. This agrees with similar observations seen during previous work **[6]**. Water lubrication greatly reduced the wear rate of both wheel and rail discs. However, test durations were kept below the rolling contact fatigue life of the rail disc. After this life has been exceeded it is likely that the rail disc would suffer severe pitting or spalling causing a large increase in wear rate and lead to a decreased contact area at the disc interface. This in turn would lead to an increased wheel disc wear rate.

As slip was increased, however, the wear rate levelled and then increased again rapidly at very high values of slip, indicating that as the severity of the contact is increased different wear regimes were apparent (*mild*, *severe* and *catastrophic*) (see Figure 6).

3.3 Wear Surface Appearance

At low slip, in the mild wear regime, oxidative wear was seen to occur on both wheel and rail discs. The disc surfaces turned a rusty brown colour. Closer examination of the wear surface of the wheel disc revealed abrasive score marks and evidence of the oxide layer breaking away from the surface (see Figure 7). This ties in with observations made in the field that on straight track where low slip occurs on the high rail, oxidative wear is prevalent generating magnetite (Fe_3O_4) **[18]** and in full-scale test-rig results, where reddish oxide film appeared for low slip conditions **[12]**.

As slip was increased, the wear mechanism of the wheel discs altered. The wheel disc appeared to be wearing by a ratchetting process (deformation followed by crack growth and subsequent material removal). Closer examination of the wheel disc surfaces revealed that this was the case (see Figure 8).

3.4 Sub-surface Morphology

Figure 9 shows a section through a wheel disc, run at low slip, parallel to the rolling direction. At the surface the oxide layer is just visible. There is a very small amount of deformation just below the wear surface of the disc.

At higher levels of slip, observation of the subsurface morphologies revealed that a larger amount of plastic deformation was occurring below the wheel disc wear surface (see Figure 10) and crack formation just below the surface was visible which was leading to thin slivers of material breaking away from the surface.

As slip was increased further far greater cracking was visible at the wear surface and some of these cracks were seen to alter direction from running parallel to the wear surface and turning up to turning down into the material causing larger chunks of material to break away (see Figure 11).

4 WEAR TRANSITIONS

Figure 12 shows how the different wear features observed relate to the wear rates and regimes observed in the results of the twin disc testing.

The data indicates that transitions occur in the wear regimes. At low slip wear appears to be dominated by surface oxidation. This is commonly called the mild wear regime and has been

observed by a number of researchers **[3, 4, 19]**. At high slip the wear is dominated by surface cracking and mass loss by spalling. This regime has been less well observed **[6]** and is sometimes called the catastrophic wear regime. For the data of the present experiments, the transitions between these regimes is studied in more detail. It is proposed that the first transition is associated with the onset of fully sliding contact conditions and the second is a result of surface temperature effects.

4.1 Friction versus Slip in the Twin Disc Contact

Figure 13 shows friction measurements taken during the wear tests carried out at 1500MPa plotted against slip. As would be expected the friction reaches a threshold. This transition represents the change from partial slip in the disc interface to full slip conditions. Also shown is the Carter creep curve for an assumed limiting friction of 0.5. This model creep curve is based on smooth elastic cylinders in contact **[20]**.

The wear data (also shown in Figure 13) follows a similar pattern indicating that at the point of transition from partial slip to full slip a wear transition also occurs. After the full slip condition has been reached, increasing the magnitude of slip has no effect.

As slip is increased the traction distribution, q, in the contact increases (whilst $q<\mu p$). The shear stress at the surface thus increases, which results in increasing wear with slip. Once limiting friction has been reached ($q=\mu p$ everywhere in the contact region) then the surface shear stress remains constant with increasing slip. This explains the plateau shown in Figure 13. The wear is largely independent of sliding velocity. This is an interesting observation because it suggests that, in this regime, the wear is controlled by contact stress and limiting traction alone. If the wear mechanism had been by abrasion (for example caused by asperities or hard particles abrading the surface) then increasing the sliding velocity would result in

proportionally more abrasive ploughing and wear. In this regime it is therefore reasonable to model the material removal process using a contact mechanics model such as those proposed previously **[21]**. The contact stress causes an increment of shear strain, which accumulates (ratchets) until the material ruptures **[22]**.

At the second wear transition (where the wear data breaks from the pattern of the friction measurements) some other mechanism must occur, leading to the much higher wear rates observed.

4.2 Twin Disc Contact Temperature

Once the slip has reached about 15% the wear rate increases rapidly. The theoretical smooth surface stress state, however, remains unaltered since the normal load and traction coefficient are unchanged. Clearly the increase in sliding speed has resulted in some mechanism changes. In this section the associated surface temperature rise is considered.

An approach for determining the temperature in a twin disc experimental contact has been outlined previously **[23]**. The work described was focussed on discs made from polymers, the same basic approach is used here, but for wheel and rail steel discs.

The disc surface temperature is made up of three components:

1. The body temperature, T_b, of the material under the contacting surfaces of the discs, which is the average temperature of the outer surface of the discs.
2. The instantaneous temperature rise above the bulk temperature at the point of contact, called the flash temperature, T_f **[24]**.
3. The ambient temperature of the air surrounding the discs, T_a.

4.2.1 Body Temperature

In order to calculate the body (or average surface temperature) of the two discs in contact, T_b, heat generated due to sliding friction in the contact is equated to heat loss due to convection, conduction and radiation giving:

$$\mu F_n u_s = 2\left(\dot{Q}_1 + \dot{Q}_2 + \dot{Q}_3\right) \quad (1)$$

where μ is the coefficient of friction, F_n is the normal load applied to the discs, u_s is the sliding speed and $\dot{Q}_1$, $\dot{Q}_2$ and $\dot{Q}_3$ are heat loss due to convection, conduction and radiation respectively. The dissipated heat is multiplied by two as there are two discs. Actual measured friction data is used in equation (1). A change in roughness of the disk surfaces would be expected to change the friction and hence the heat generation. By using measured friction data it is not necessary to know the relationship between roughness and heat generation.

The heat loss due to convection is obtained by assuming that a laminar thermal boundary layer exists at the disc surface. As the layer reaches the disc interface it is removed (to then reform on the subsequent disc rotation). The rate of heat loss as the thermal layer is removed gives the heat loss due to convection and can be expressed as **[25]**:

$$\dot{Q}_1 = 0.664 b k_a \left(T_b - T_a\right) \sqrt[3]{\frac{\eta_a C_p}{k_a}} \sqrt{\frac{u_r L_d \rho_a}{\eta_a}} \quad (2)$$

where b is the contact width of the discs, k_a is the thermal conductivity of air (0.025 W/m/K), η_a is the dynamic viscosity of air (2×10^{-5} kg/m/s), C_p is the specific heat capacity of air (1 kJ/kg/K), u_r is the air velocity relative to the disc (equal to the disc surface speed), L_d is the disc circumference, ρ_a is the density of air, T_a is the ambient air temperature and T_b is the disc body temperature.

In calculating heat dissipated due to conduction it is assumed that heat only flows in a radial direction within the disc. Fourier's law is applied and the dissipated heat is given by (for example see **[26]**):

$$\dot{Q}_2 = 2\pi r b k_s \frac{dT}{dR} \tag{3}$$

where r is the radius at any point within the disc, k_s is the thermal conductivity of the wheel steel and dT/dR is the thermal gradient in the radial direction.

If r_o is the disc outer radius and r_i and T_i are the disc inner radius and temperature, the following boundary conditions can be applied; $T = T_b$ when $r = r_o$, and $T = T_i$ when $r = r_i$. Equation 3 can then be integrated to give:

$$\dot{Q}_2 = \frac{2\pi b k_s}{\ln\left(\frac{r_o}{r_i}\right)}\left(T_b - T_i\right) \tag{4}$$

T_i was assumed to be equal to the temperature of the disc shaft, which was measured during the wear tests.

The heat dissipated due to radiation is given by (for example see **[27]**):

$$\dot{Q}_3 = \sigma A_d \varepsilon_{rad}\left(T_b^4 - T_a^4\right) \tag{5}$$

where σ is the Stefan-Boltzmann constant (5.669×10^{-8}W/m^2/K), ε_{rad} is the emissivity of the disc steel and A_d is the area of the disc dissipating radiation energy.

The area A_d was taken as $5\pi r_o b/3$ (i.e. it is assumed that 300° of each disc is radiating heat to the surrounding air and 60° on each is radiating heat to the other disc, as shown in Figure 14). Heat loss from the sides of the discs was neglected.

Substituting Equations 2, 4 and 5 into Equation 1 enables the body temperature, T_b, to be calculated, as it is the only unknown.

4.2.2 Flash Temperature

Expressions for flash temperature in line contacts for various velocity ranges have been summarised previously **[28]**. The formula to be used varies with the Peclet number, L, given by:

$$L = \frac{Ua}{2\chi} \tag{6}$$

where U is the velocity of either contacting solid, a is the contact half width and χ is the thermal diffusivity given by:

$$\chi = \frac{k_s}{\rho C_{p_s}} \tag{7}$$

where ρ is the density of the wheel/rail steel and C_{p_s} is the specific heat capacity of the wheel/rail steel.

For the twin disc contact L is 10.3 (U = 0.98m/s; a = 3150μm; k_s = 60W/m/K; ρ = 8000kg/m^3, C_{p_s} = 500J/kg/K).

For L>5, average and maximum flash temperatures for a line contact are given by **[28]**:

$$\overline{T}_f = 1.064 \frac{\dot{q}}{k_s}\left(\frac{\chi a}{U}\right)^{0.5} \text{ and } \hat{T}_f = \frac{2\dot{q}}{k_s}\left(\frac{2\chi a}{\pi U}\right)^{0.5} \tag{8}$$

where $\dot{q}$ is the rate of heat supply per unit area given by:

$$\dot{q} = \frac{\dot{Q}}{2ab} \tag{9}$$

where Q is the generated heat ($\mu F_n v_s$) and b is the contact length.

The heat generated in frictional contacts is split between the contacting solids. The proportion of the total heat flowing to each body is determined on the basis that the average surface temperature is the same for both bodies. A simple way to estimate the *true* temperature rise is to assume that all the heat generated is supplied to body A. The appropriate calculation should then be carried out to obtain the flash temperature in solid A, $T_{f\mathrm{A}}$. It should then also be carried out assuming that all the heat is supplied to body B to obtain $T_{f\mathrm{B}}$. The true average and maximum flash temperature rises must be the same for both solids in contact and are given by:

$$\frac{1}{\overline{T}_f} = \frac{1}{\overline{T}_{f\mathrm{A}}} + \frac{1}{\overline{T}_{f\mathrm{B}}} \text{ and } \frac{1}{\hat{T}_f} = \frac{1}{\hat{T}_{f\mathrm{A}}} + \frac{1}{\hat{T}_{f\mathrm{B}}} \tag{10}$$

4.2.3 Total Contact Surface Temperature

The total surface temperature T_{tot}, is given by:

$$T_{tot} = T_b + T_f \tag{11}$$

Calculations were carried out to determine total temperatures in the disc contact for the range of conditions used during the wear testing (see Table 1). Table 3 shows the results of calculations carried out for tests run at 1500MPa (7.4kN) with a nominal disc speed of 400rpm (surface velocity 0.98m/s). Friction coefficients used in calculating the heat generated were those measured during the tests.

The average and maximum total temperatures for the 1500MPa wear tests are shown plotted against slip in Figure 15.

Comparison of temperature data with wear data (also shown in Figure 15) indicates that the second wear transition occurs at disc temperatures of 200-250°C. Yield stress data for steels similar to the wheel material indicates that a drop occurs at around 200-300°C **[29]**.

Numerical calculations carried out to determine temperatures in an actual wheel/rail contact **[30, 31]** have indicated that for similar contact conditions, temperatures of a similar order of magnitude are obtained. For example, temperatures have been calculated from 280°C to 700°C for slips of 8% to 20% **[31]**. In this case the wheel speed, and hence sliding velocity in the contact, is much higher than in the twin disc contact, which means there is greater heat generation. There is, however, a much larger volume of material in which to dissipate the heat and the wheel is always contacting with cold rail, leading to similar temperatures to those apparent in the twin disc contact. It would appear, therefore, that it is possible to achieve similar temperatures in the wheel rail contact and thermal wear transitions may also occur. The twin disk simulation can be used to examine what happens to the wear rate at extreme contact conditions; but this can only be translated to the wheel/rail case when the contact conditions and heat generation are fully defined.

5 DISCUSSION

In previous work an energy approach has been adopted in the analysis of the relationship between wear rate and contact conditions **[3, 4, 6]**. It was shown that wear rate (μg/m rolled/mm^2 contact area) is a linear function of wear index $T\gamma/A$ for the severe wear regime described earlier **[6]**, where T is the tractive force, γ is the slip and A is the contact area.

If the wear data from the present study is presented using this approach, at low $T\gamma/A$ conditions this relationship holds (see Figure 16). However, as shown in Figures 17a and b,

increasing the severity of the contact conditions causes the relationship to break down, as the transitions in wear rate occur.

It is clear again, though, from the comparison with wear data for existing wheels steels also shown in Figure 17 that, as indicated in Figure 4, R8T offers improved wear resistance.

Results of analysis of the wear transitions indicates that the relationship holds while partial slip conditions exist in the contact. When full slip conditions occur wear rate levels off despite increasing slip values.

Further increases in the slip value then leads to temperatures in the contact that could cause a reduction in the wheel steel material properties, which could explain the subsequent increase in wear rate. This ties in with traditional theories of pure sliding wear that suggest that different wear mechanisms occur due to thermally induced changes in the properties of the surface layer material affected **[32, 33, 34, 35]**. It has been acknowledged that studies of wear types in rolling/sliding contacts have been carried far enough to draw such conclusions **[36]**, so this work may act to fill this gap.

Most work on wear predictions in wheel/rail systems relies on a wear coefficient approach, for example the wear index, $T\gamma A$ **[6, 37]**, the friction specific wear ratio **[19]** and the Archard wear coefficient **[2]**. It is clear from these studies that it is not possible to find unique wear coefficients that cover the whole operating regime of a wheel/rail contact. Nevertheless these concepts are still useful, particularly when contact parameters can be easily calculated from the results of multi-body dynamics simulations. To get around the changes in wear rate, it is possible to assign different wear coefficients to each wear regime **[37]**. It can be seen, however, from the temperature calculations, the second wear transition is likely to move if the absolute disc velocity is changed, so at high $T\gamma A$ values the approach may not be valid. A wear index based solely on sliding velocity or distance will thus not work adequately.

This improved understanding will help in the progressing towards the aim of eventually attaining a wear modelling methodology reliant on material properties rather than wear constants derived from testing.

6 CONCLUSIONS

- Twin disc wear testing has been carried out to study the wear characteristics of R8T railway wheel steel.
- The results have indicated that compared to previous wheel steels R8T offers greater wear resistance, while not increasing the wear rate of the rail material.
- Three wear regimes were identified for R8T; *mild*, *severe* and *catastrophic*. These were classified in terms of wear rate and features. Mild wear was characterised by low wear rates and oxidative wear. Increasing the severity of the contact led to cracking
- Analysis of the contact conditions in terms of friction and slip indicated that the levelling off of the wear rate observed at the first wear transition was caused by the change from partial slip to full slip conditions at the disc interface. Temperature calculations for the contact showed that the large increase in wear rates seen at the second wear transition may result from a thermally induced reduction in yield strength and other material properties.

7 ACKNOWLEDGEMENTS

The work reported in this paper was carried out as part of the European Community funded project HIPERWheel (contract number: G3RD-CT2000-00244).

8 REFERENCES

1 **Stanca, M., Stefanini, A., Gallo, R.** Development of an integrated design methodology for a new generation of high performance rail wheelsets. *Proceedings of the 16th European MDI User Conference*, Berchtesgaden, Germany, 14-15 November, 2001.

2 **Jendel, T.** Prediction of wheel profile wear - comparisons with field measurements. *Proceedings of the International Conference on Contact Mechanics and Wear of Rail/Wheel Systems*, Tokyo, Japan, 25-28 July, 2000, 117-124.

3 **Beagley, T.M.** Severe wear of rolling/sliding contacts. *Wear*, **36**, 1976, 317-335.

4 **Bolton, P.J., Clayton, P., McEwen, I.J.** Wear of rail and tyre steels under rolling/sliding conditions. *ASLE Transactions*, 1982, **25**(1), 17-24.

5 **Kumar, S., Rao, D.L.P.** Wheel-rail contact wear, work, and lateral force for zero angle of attack - a laboratory study. *Transactions of the ASME, Journal of Dynamic Systems, Measurement, and Control*, 1984, **106**, 319-326.

6 **Bolton, P.J., Clayton, P.** Rolling-sliding wear damage in rail and tyre steels. *Wear*, 1984, **93**, 145-165.

7 **Fries, R.H., Dávila, C.G.** Wheel wear predictions for tangent track running. *Transactions of the ASME, Journal of Dynamic Systems, Measurement, and Control*, 1987, **109**, 397-404.

8 **Pearce T.G., Sherratt N.D.** Prediction of wheel profile wear. *Wear*, 1991, **144**, 343-351.

9 **Zobory, I.** Prediction of wheel/rail profile wear. *Vehicle System Dynamics*, 1997, **28**, 221-259.

10 **Dearden, J.** The wear of steel rails and tyres in railway service. *Wear*, 1960, **3**, 43-49.

11 **Steele, R.K.** Observations of in-service wear of railroad wheels and rails under conditions of widely varying lubrication. *ASLE Transactions*, 1982, **25**(3), 400-409.

12 **McEwen, I.J., Harvey, R.F.** Full-scale wheel-on-rail testing: comparisons with service wear and a developing theoretical predictive model. *Lubrication Engineering*, 1985, **41**(2), 80-88.

13 **Krause, H., Poll, G.** Wear of wheel-rail surfaces. *Wear*, 1986, **113**, 103-122.

14 **Garnham, J.E., Beynon, J.H.** Dry rolling-sliding wear of bainitic and pearlitic steels. *Wear*, 1992, **57**, 81-109.

15 **Garnham, J.E., Beynon, J.H.** The early detection of rolling-sliding contact fatigue cracks. *Wear*, 1991, **144**, 103-116.

16 **Fletcher, D.I., Beynon, J.H.** Development of a machine for closely controlled rolling contact fatigue and wear testing. *Journal of Testing and Evaluation*, 2000, **28**(4), 267-275.

17 **Tyfour, W.R., Beynon, J.H., Kapoor, A.** The steady state wear behaviour of pearlitic rail steel under dry rolling-sliding contact conditions. *Wear*, 1995, **180**, 79-89.

18 **Broster, M., Pritchard, C., Smith, D.A.** Wheel-rail adhesion: it's relation to rail contamination on British railways. *Wear*, 1974, **29**, 309-321.

19 **Deters, L., Proksch, M.** Friction and wear of rail and wheel material. *Proceedings of CM2003, 6th International Conference on Contact Mechanics and Wear of Rail/Wheel Systems*, 2003, **1**, 175-181.

20 **Carter, F.W.** On the action of a locomotive driving wheel. *Proceedings of the Royal Society*, 1926, **A112**, 151-157.

21 **Bower, A.F., Johnson, K.L.** Plastic flow and shakedown of the rail surface in repeated wheel-rail contact. *Wear*, 1991, **144**, 1-18.

22 **Kapoor, A.** A Re-evaluation of the life to rupture of ductile metals by cyclic plastic strain. *Fatigue and Fracture of Engineering Materials and Structures*, 1994, **17**, 201-219.

23 **Kukureka, S.N., Chen, Y.K., Hooke, C.J., Liao, P.** The wear mechanisms of acetal in unlubricated rolling-sliding contact. *Wear*, 1995, **185**, 1-8.

24 **Blok, H.** The flash temperature concept. *Wear*, 1963, **6**, 483-494.

25 **Young, A.D.** *Boundary Layers*, Blackwells, Oxford, 1989.

26 **Simonson, J.R.** *Engineering Heat Transfer*. Macmillan Press, Hong Kong, 1975.

27 **Holman, J.P.** *Heat Transfer*. 9th Edition, McGraw-Hill, London, 2002.

28 **Jaeger, J.C.** Moving sources of heat and the temperature at sliding contacts. *Proceedings of the Royal Society, N.S.W.*, 1943, **76**, 203-224.

29 **British Steel Makers Creep Committee** *BSCC High Temperature Data*. The Iron and Steel Institute for the BSCC, London, 1973.

30 **Ertz, M, Knothe, K.** A comparison of analytical and numerical methods for the calculation of temperatures in wheel/rail contact. *Wear*, 2002, **253**, 498-508.

31 **Gupta, V., Hahn, G.T., Bastias, P.C., Rubin, C.A.** Calculations of the frictional heating of a locomotive wheel attending rolling plus sliding. *Wear*, 1996, **191**, 237-241.

32 **Ling, F.F., Saibel, E.E.** Thermal aspects of galling of dry metallic surfaces in sliding contact. *Wear*, 1957, **1**, 80-91.

33 **Rozeanu, L.** A model for seizure. *ASLE Transactions*, 1973, **16**, 115-120.

34 **Lim, S.C., Ashby, M.F.** Wear Mechanism Maps. *Acta Metallica*, 1987, **35**, 1-24.

35 **Ludema, K.C.** Mechanism-based modelling of friction and wear, *Wear*, 1996, **200**, 1-7.

36 **Markov, D., Kelly, D.** Mechanisms of adhesion-initiated catastrophic wear: pure sliding. *Wear*, 2000, **239**, 189-210.

37 **Lewis, R., Braghin, F., Ward, A., Bruni, S., Dwyer-Joyce, R.S., Bel Knani, K., Bologna, P.** Integrating dynamics and wear modelling to predict railway wheel profile evolution. *Proceedings of CM2003, 6th International Conference on Contact Mechanics and Wear of Rail/Wheel Systems*, 2003, **1**, 7-16.

Figure Titles

Figure 1

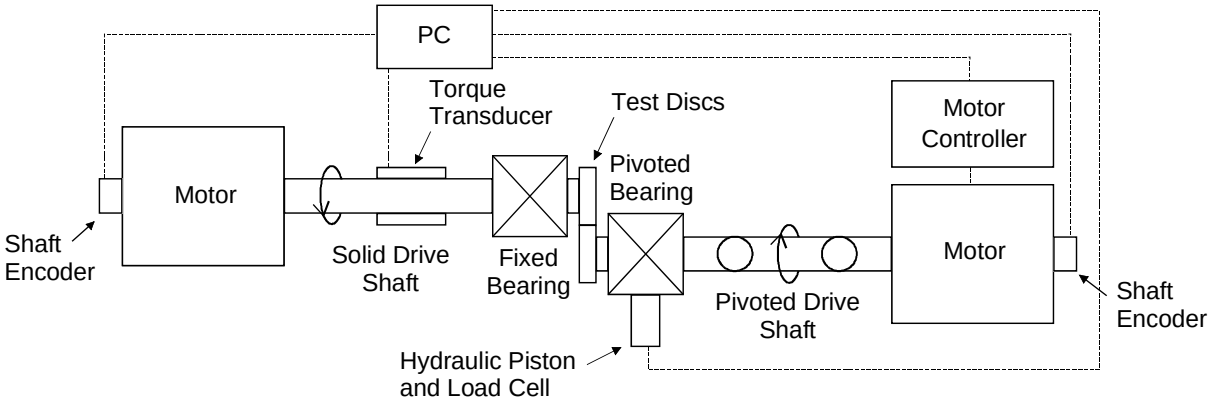

Figure 2

Figure 3

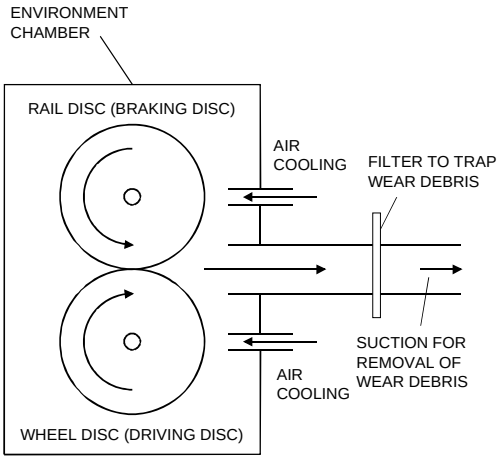

Figure 4

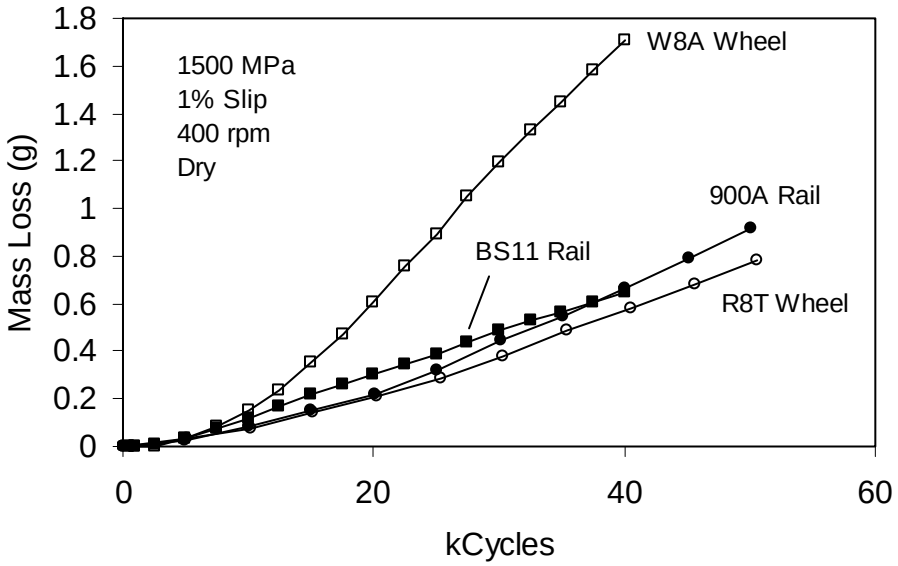

Figure 5

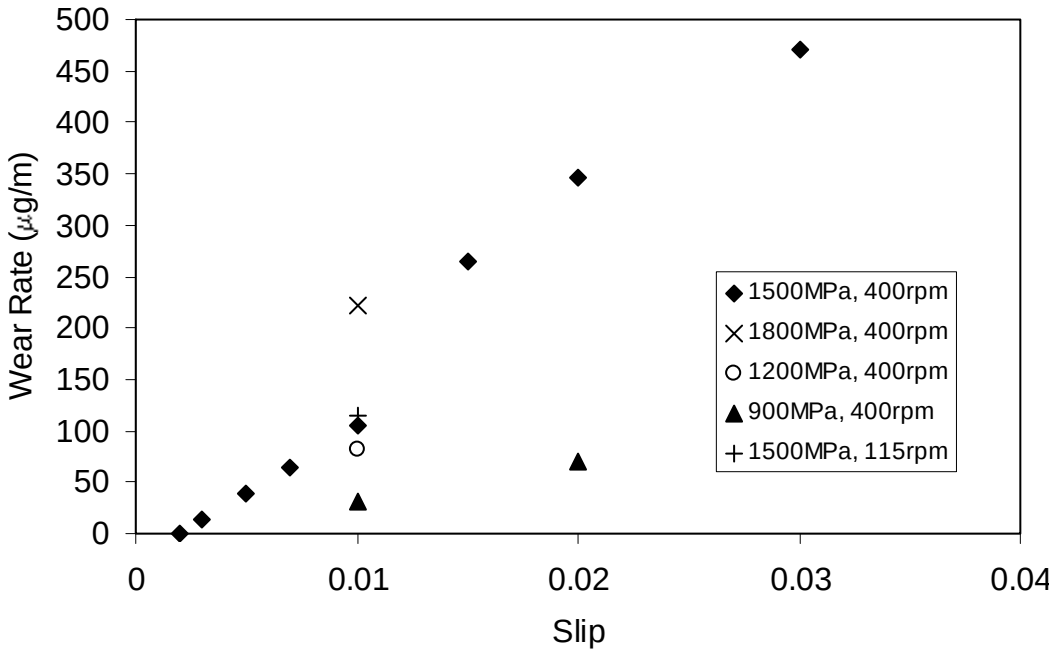

Figure 6

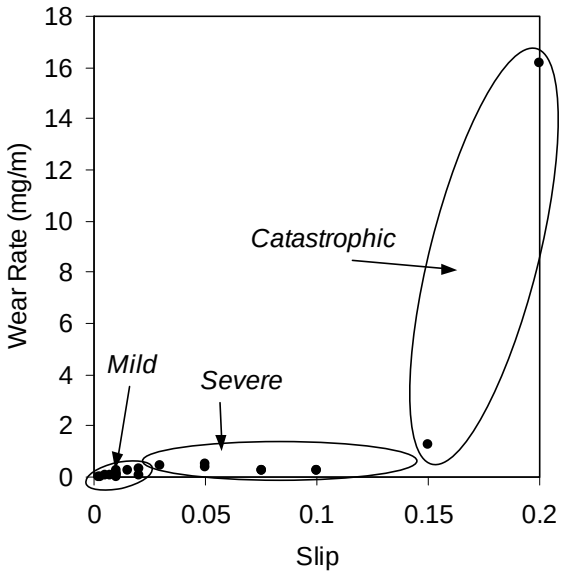

Figure 7

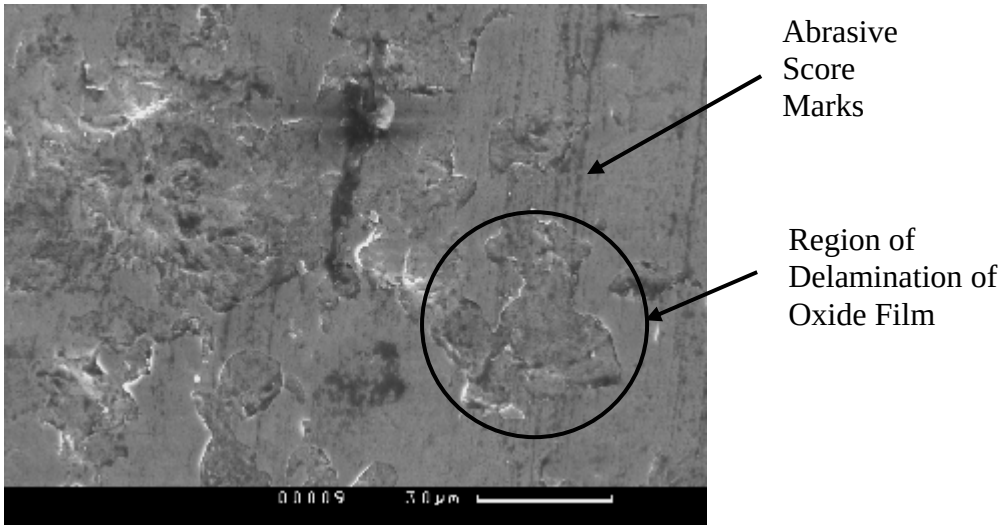

Figure 8

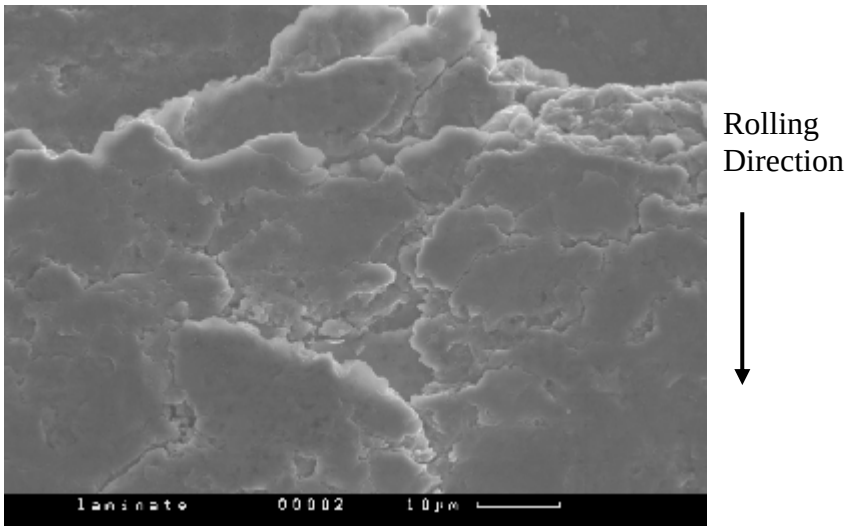

Figure 9

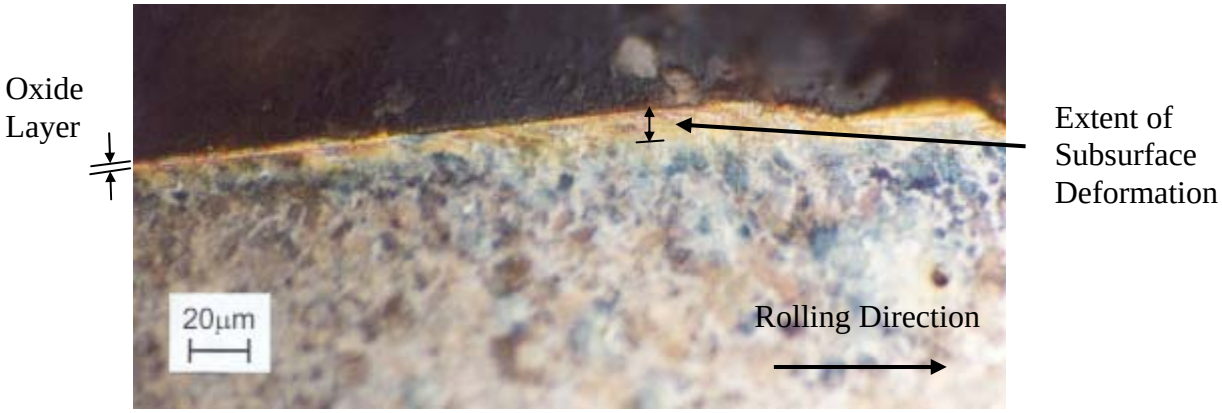
Oxide
Layer
Extent of
Subsurface
Deformation
20μm
Rolling Direction

Figure 10

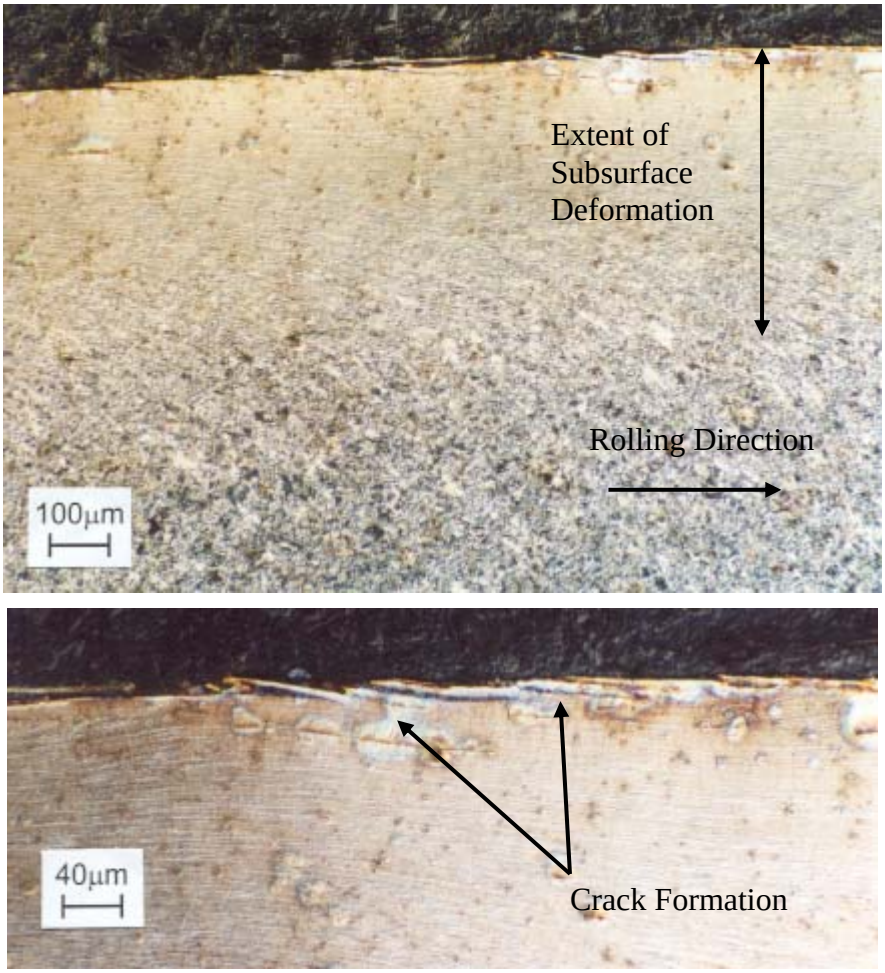
Extent of
Subsurface
Deformation
Rolling Direction
100µm
40µm
Crack Formation

Figure 11

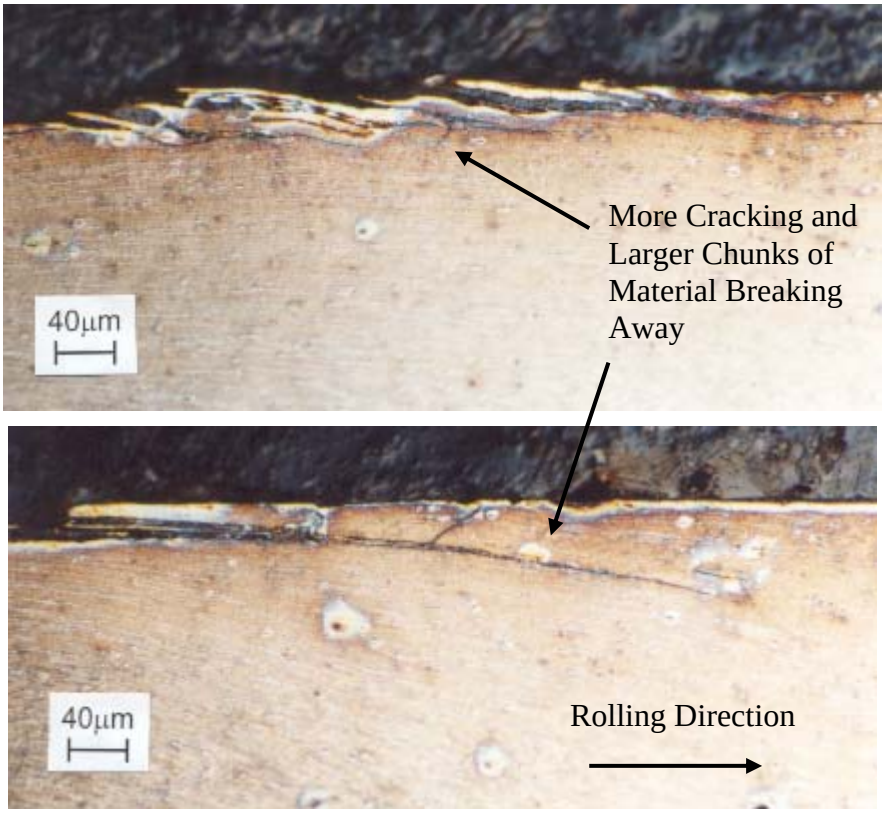

Figure 12

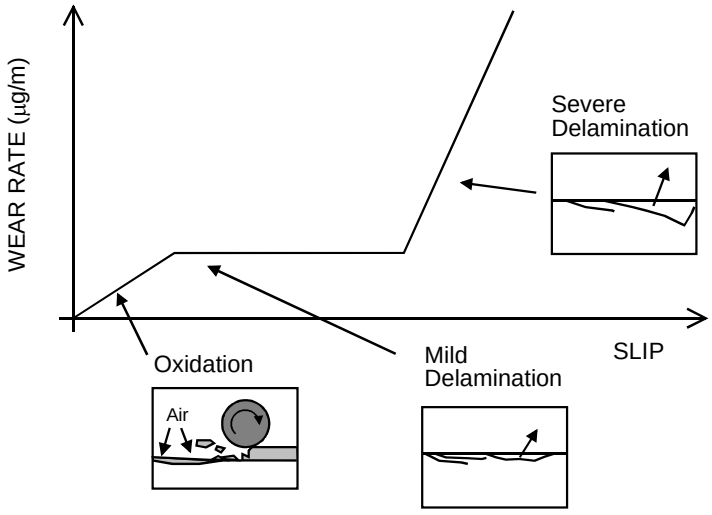

Figure 13

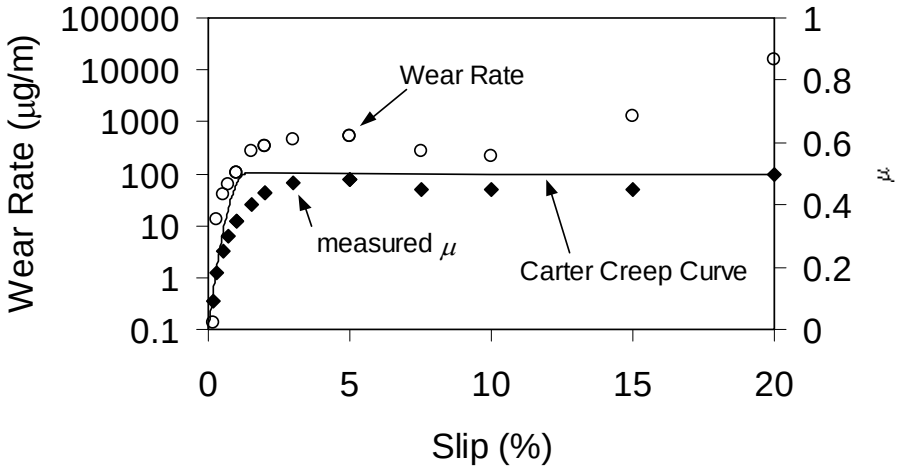

Figure 14

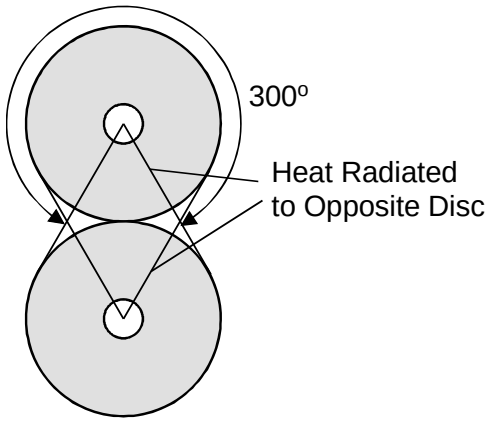

Figure 15

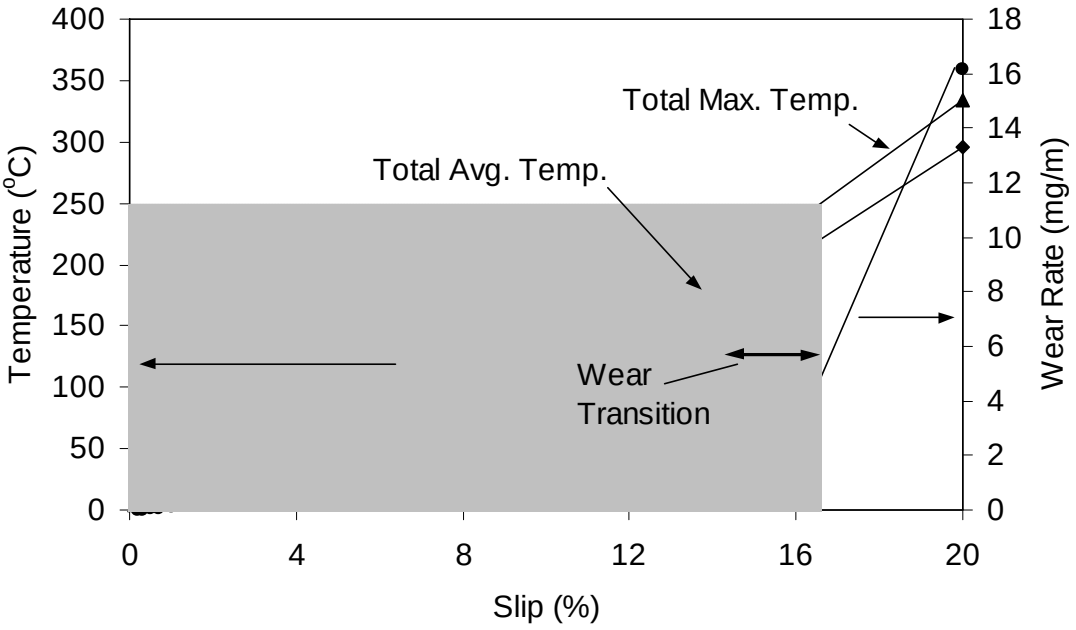

Figure 16

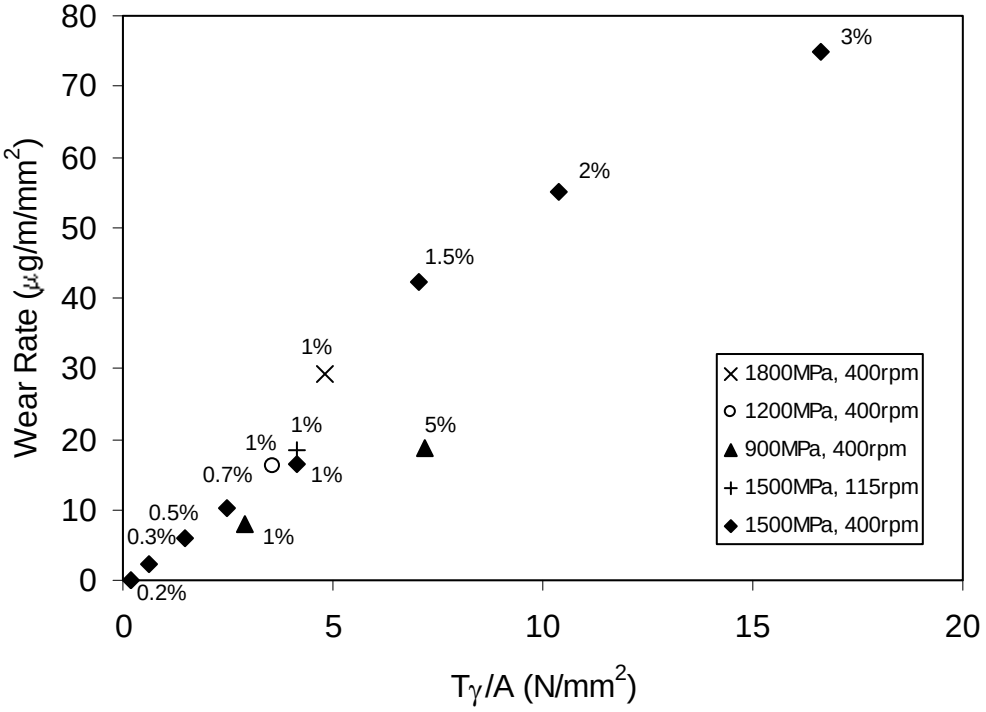

Figure 17

(a)

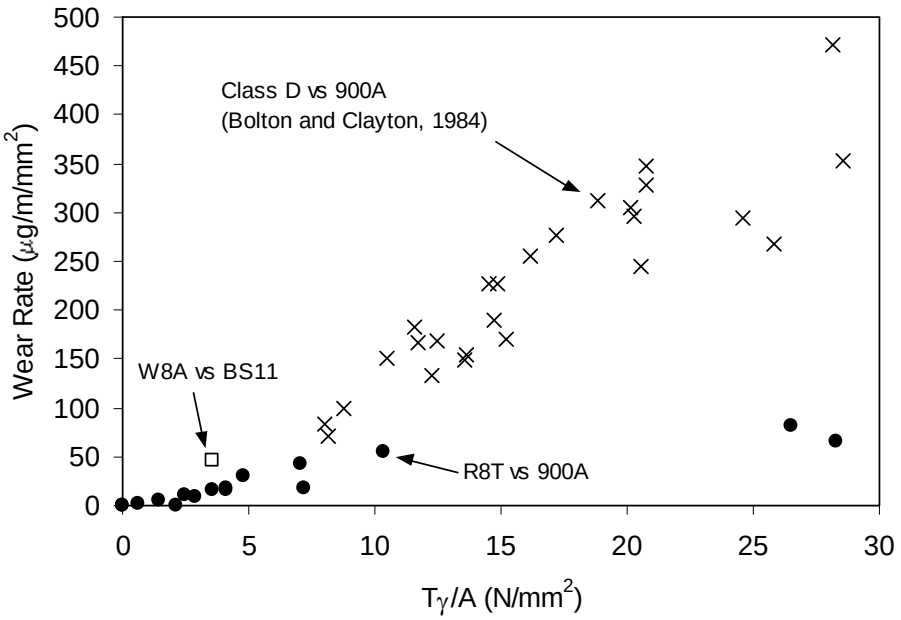
Class D vs 900A
(Bolton and Clayton, 1984)
W8A vs BS11
R8T vs 900A
Wear Rate (μg/m/mm²)
Tγ/A (N/mm²)
0
50
100
150
200
250
300
350
400
450
500
0
5
10
15
20
25
30

(b)

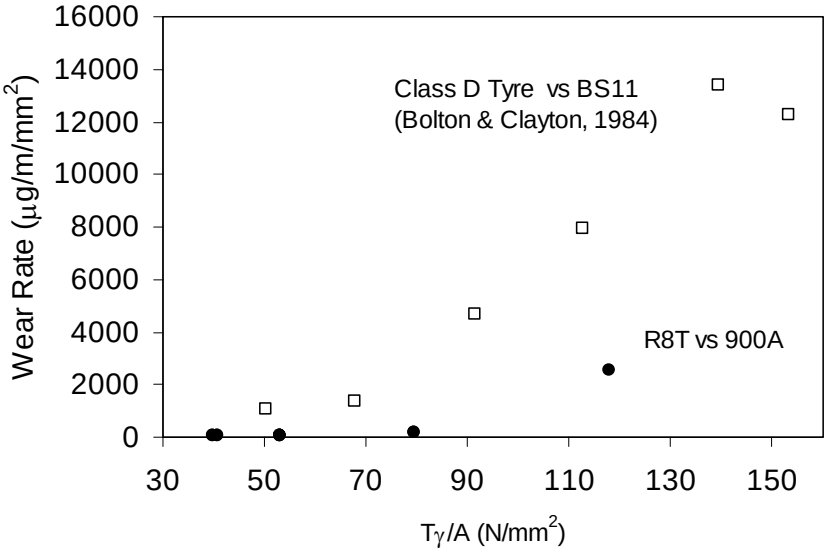
Class D Tyre vs BS11
(Bolton & Clayton, 1984)
R8T vs 900A
Wear Rate (μg/m/mm²)
Tγ/A (N/mm²)
0
2000
4000
6000
8000
10000
12000
14000
16000
30
50
70
90
110
130
150

Table 1

Contact Press. (MPa)	Slip (%)	Nom. Speed (rpm)	Lubn.	Nom. Cycles
1500	0.2	400	No	50000
1500	0.3	400	No	50000
1500	0.5	400	No	50000
1500	0.7	400	No	50000
900	1	400	No	50000
1200	1	400	No	50000
1500	1	400	No	50000
1800	1	400	No	50000
1500	1	115	No	50000
1500	1.5	400	No	50000
900	2	400	No	50000
1500	2	400	No	50000
1500	3	400	No	50000
1500	5	400	No	50000
1500	7.5	400	No	50000
1500	10	400	No	50000
1500	15	400	No	1000[1]
1500	20	400	No	1000[1]

[1]Tests at high slip conditions were run for shorter durations due to the rapid heat generation and unstable wear experienced under these conditions.

Table 2

Material	Hardness (GPa)
W8A (wheel)	2.7
BS11 (rail)	2.45
R8T (wheel)	2.6
900A (rail)	2.65

Table 3

Slip (%)	Heat Generated (W)	Proportion of Heat Dissipated (%)			T_b (°C)	$\overline{T}_f$ (°C)	$\hat{T}_f$ (°C)	$\overline{T}_{tot}$ (°C)	$\hat{T}_{tot}$ (°C)
		Cond.	Conv.	Rad.					
0.2	1.3	0.924	0.076	4×10^{-6}	20.6	0.13	0.19	20.7	20.8
0.5	9.2	0.948	0.052	3×10^{-6}	22.9	0.9	1.3	23.8	24.2
1	25.7	0.950	0.049	4×10^{-6}	27.5	2.5	3.7	30	31.2
3	102.6	0.953	0.047	1.4×10^{-5}	48.6	10.1	15.1	58.7	63.7
7.5	246.0	0.952	0.047	6.5×10^{-5}	89.0	24.4	36.7	113.4	125.7
10	327.8	0.952	0.048	1.2×10^{-4}	111.9	32.8	49.2	144.7	161.1
15	492.1	0.960	0.040	1.6×10^{-4}	136.8	49.9	74.8	186.7	211.6
20	728.4	0.952	0.047	8.2×10^{-4}	220.9	75.0	112.5	277.1	314.6